Tunnelling and Underground Space Technology 84 (2019) 373–380

Contents lists available at ScienceDirect

Tunnelling and Underground Space Technology

journal homepage: www.elsevier.com/locate/tust

Transverse extent of numerical model for deep buried tunnel excavation

Kai Su[a,*], Yan-Jun Zhang[a], Zhi-Hui Chang[b,a], He-Gao Wu[a], Tao Wang[a], Wei Zhou[a]

[a] State Key Laboratory of Water Resources and Hydropower Engineering Science, Wuhan University, Wuhan 430072, China
[b] Shanghai Municipal Engineering Design Institute (Group) Co., Ltd, Shanghai 200092, China

ARTICLE INFO

Keywords:
Tunnel excavation
Numerical model
Model extent
FLAC^{3D}

ABSTRACT

Numerical simulation has been widely used for predicting rock mass convergence during tunnel excavation. Considering that tunnel construction is a three-dimensional (3D) process, the 3D numerical analysis, instead of the plane-strain models, are commonly employed in engineering practice. As the 3D numerical analyses require large numbers of computational resources, the geometric extents are often kept to a minimum to reduce simulation time. However, there is a lack of published information concerning appropriate the size of numerical model. The study investigates how the transverse range of tunnel section, including the upper boundary, the lower boundary and the lateral boundary, affects the tunnel convergence via the finite difference software package FLAC^{3D}, respectively. Then, a comprehensive function to yield the minimum transverse section area within a given error is proposed. After several cases with different categories of rock are employed in the simulations, the universal model extents with the minimum transverse section area are proposed.

1. Introduction

Numerical analysis is one of the most popular and powerful way to deepen the understanding of the real world in the history of engineering and sciences (Cai, 2008). Numerical analysis can be used in tunnel design to reduce the fracture and failure in all types of tunnels as well as control and reduce the risk of tunnel construction failures. Numerical analysis is a very economical, popular and capable method of predicting the behavior of tunnel structures at different loading conditions. Many material models such as Mohr-Coulomb, Hoek-Brown and Drucker-Prager failure criteria for geotechnical medium have been provided by commercial codes. The most widely used codes are FLAC3D, ABAQUS, PLAXIS, CRISP, FEM3D as well as LUSAS, which have powerful and versatile post-processing modules. As shown in Table 1, there are numerous researches about simulating tunnel excavation with the application of the numerical calculation software. And accessible user interface in these numerical tools has made it possible for someone with or without strong knowledge background of numerical modeling theory to conduct a tunnel excavation analysis in just a few minutes. However, some users of these numerical tools are lack of a complete understanding of the solution schemes and models adopted in these codes. It is effective to organize the professional training for the beginners. Studying the classical cases and using the numerical software to validate cases are also helpful.

Compared with the plane-strain model, the three dimensional numerical analysis is more accurate to mimic the process of tunnel construction and prevalent in engineering practice. It is acknowledged that there are errors on the results of the section in close proximity to the model's boundary. From the view of achieving steady-state, the numerical model of tunnel should be constructed over as long a proper distance as possible to avoid the unnecessary boundary effect. For instance, Zhao et al. (2012) suggested the mesh in the transversal plane should be built by an expansion factor of 10 in relation to the tunnel diameter, D, for squeezing conditions, this factor should be increased to $15D$. However, it is likely to result in the large-scale numerical model, such as more than $20D$ of the model extent, with million grids (Liu et al., 2009). As there are limitations on computational time and resources with the growing number of elements, the geometric extents are often kept to a minimum to reduce computational time. And the majority of researches about the geometric extent focused on the influence of the longitudinal extent. (Su et al., 2016; Franzius et al., 2005; Vermeer et al., 2002). It is universally acknowledged that the transverse extent has dramatic influence on the numerical results, while there are inadequate studies in unifying the criteria for determining the transverse extent. Lambrughi et al.(2012) advised $(H + 4D)$ for the mesh height as well as $2(H + 4D)$ for the mesh width, where H is the cover of the tunnel and D is the tunnel diameter. Most researches for tunnel excavation about how to determine the transverse extent of the numerical model are based on the researcher's own judgment rather than a uniform standard. As shown in Table 1 and Fig. 1, the width of the

* Corresponding author.
E-mail address: suker8044@163.com (K. Su).

https://doi.org/10.1016/j.tust.2018.11.034
Received 20 February 2017; Received in revised form 7 September 2018; Accepted 24 November 2018
Available online 29 November 2018
0886-7798/

Table 1
Parameters of some numerical models with diverse software package.

Authors	Material	D/m	H_1/m	H_2/m	H_3/m	K	Program
Katzenbach et al. (1981)*	Nonlinear elastic	6.7	15.2 2.27D	–	35 5.22D	0.8	–
Lee et al. (1991)#	Elastic perfectly plastic transverse anisotropic	2.5	8 3.20D	–	19.5 7.80D	0.85	FEM3D
Burd et al. (2000) and Augarde et al. (1998)#	Nonlinear elastic plastic	5	10 2.00D	50 10.00D	60 12.00D	1.0	OXFEM
Dasari et al. (1996)*	Nonlinear elastic perfectly plastic (SDMCC)	8	25 3.13D	25 3.13D	40 5.00D	1.0	CRISP
Komiya et al. (1999)*	Elastic perfectly plastic anisotropic	3.7	33 8.92D	–	–	0.55	–
Tang et al. (2000)*	Elastic perfectly plastic transverse anisotropic	8.6	25 2.91D	–	80 9.30D	1.5	ABAQUS
Guedes et al. (2000)*	Elastic	6	9 1.50D	–	60 10.00D	0.5,1.0	ABAQUS
Dias et al. (2000)*	Elastic perfectly plastic	9.8	25 2.55D	–	–	0.36,0.43	FLAC3D
Vermeer and Bonnier et al. (2002)*	Linear elastic perfectly plastic	8	20 2.50D	8 1.00D	55 6.88D	0.67	PLAXIS
Doležalová (2002)*	Linear elastic perfectly plastic/ Nonlinear elastic perfectly plastic	3.6	15.7 4.82D	–	22 6.76D	0.5–1.5	CRISP
Lee et al. (2002)*	Elastic perfectly plastic	9	22.5 2.50D	–	75 8.33D	0.5,1.5	ABAQUS
Shin et al. (2002)*	Elastic perfectly plastic	9.2	20 2.17D	100 10.87D	100 10.87D	0.58–0.2	ICFEP (FSAFEM)
Galli et al. (2004)*	Elastic perfectly plastic	11	11 1.00D	33 3.00D	44 4.00D	0.5	LUSAS
Franzius and Potts (2005)*	Nonlinear elastic perfectly plastic	4.15	20 4.82D	20 4.82D	100 24.10D	1.5	ICFEP
Liu and Small et al. (2009)*	nonlinear elastoplastic	10.0	15 1.5D	85 8.5D	150 30D	0–0.55,2	ABAQUS
Lambrughi and Medina Rodríguez et al. (2012)*	nonlinear elastoplastic	9.38	13.81 1.47D	37.52 4D	102.66 10.94D	–	Flac3D
Do et al. (2014)*	linear elasto-plastic	9.1	19.55 2.15D	40.45 4.45D	60 13.19D		Flac3D
Jenck et al. (2003)#	linear elasto-plastic	9.8	26 2.65D	–	100 10.2D	0.6–1.05	Flac3D
Phienwej et al. (2006)*	linear elasto-plastic	6.4	8–25 1.25–3.91D	33–50 5.16–7.81D	50 7.81D	0.5–0.75	Flac3D
Maranha et al. (2000)*	linear elasto-plastic	9.71	17 1.75D	17 1.75D	50 5.15D	0.67	–
Barla et al. (2005)*	linear elasto-plastic	7.8	15–20 1.92–2.56D	–	80 20.51D	0.5	–
Zhang et al. (2015)#	Elastic perfectly plastic	3.75–75	101.9–137.5 1.83–26.17D	–	–	0.5,1.2	Flac3D
Zhang et al. (2012)#	Elastic perfectly plastic	30	115 3.83D	–	–	–	Flac3D

Note: Empty entries: no information found.
D = tunnel diameter.
H_1 = upper height: distance between tunnel center line and model top.
H_2 = Lower height: distance between tunnel center line and model bottom.
H_3 = model half width.
K = lateral coefficient.
* Step-by-step approach.
# Plain strain analysis.

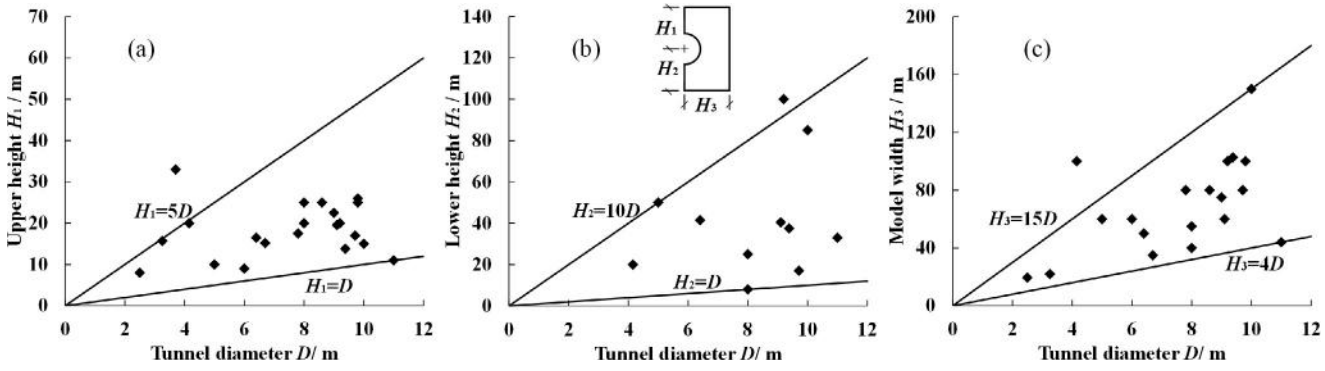

Fig. 1. Range of transverse model extent, (a) upper height, (b) lower height and (c) model half width.

numerical model, H_3, varies from 4D to 15D, the value of the lower height, H_2, varies from 1D to 10D and the value of upper height ranges from 1D to 5D. The model extents, including H_1, H_2 and H_3, exist great differences in each study and seem to be derived from the researchers' numerical experience that is commonly based on the geological conditions, the sensitivity analysis and so on, while there is no consensus on the determination of the numerical model extent.

The aim of this paper is to propose the method to determine the minimum transverse extent of numerical model with reliable accuracy for the simulation of tunnel excavation. Firstly, the development of the numerical model is reviewed. Secondly, the transverse extent of the tunnel model, consisting of the upper height, lower height and width, is analyzed about the influence on the tunnel convergence. Further, a comprehensive function to determine the minimum transverse section area is proposed. Before the end, a short discussion of the compound functions are yielded with diverse geological conditions and the universal suggestions for transverse extent are proposed for the common engineering.

2. Development of the numerical model

2.1. Computational tool

The model has been developed via the software FLAC^{3D}, which is a commercial software package developed by Itasca Consulting Group (Itasca, 2002), based on the generalized Finite Difference Method (FDM). Dynamic equations of motion are solved at each calculation step in the modes of small strain. An explicit solution scheme is adopted, together with a mixed-discretization formulation. To model the static response of a system, a relaxation scheme is used in which artificial damping is used to dissipate kinetic energy, in which details on the subject of Dynamic Relaxation can be found in Belytschko et al. (1983).

2.2. Compound failure criterion

A compound failure criterion of Mohr-Coulomb criterion with tension cutoff is employed in this paper, which is widely used in geotechnical engineering (as shown in Fig. 2).

The envelope of instability is $f(\sigma_1, \sigma_3) = 0$, and the line from A to B is defined by shear failure criterion $f^s = 0$, which is formulized as Eq. (1).

$$f^s = \sigma_1 - \sigma_3 N_\varphi + 2c\sqrt{N_\varphi} \tag{1}$$

The line from point B to point C is defined as the tension cutoff $f^t = 0$ by the tensile strength σ^t, which is formulized as Eq. (2).

$$f^t = \sigma_3 - \sigma^t \tag{2}$$

where σ_1 and σ_3 are the first and the third principal stress; φ is the friction angle; c is the cohesive strength; σ^t is the tensile strength; $N_\varphi = \frac{1+\sin\varphi}{1-\sin\varphi}$ is a constant.

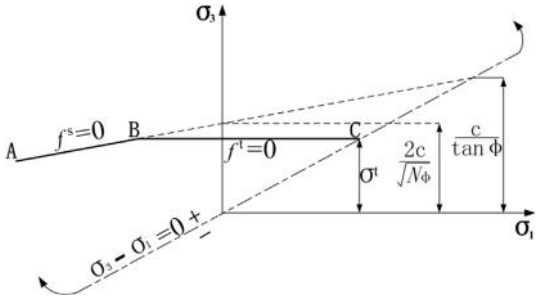

Fig. 2. Compound failure criterion (Itasca, 2002).

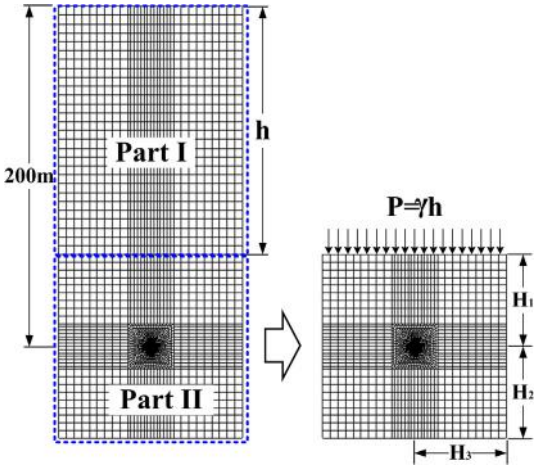

Fig. 3. Computational model.

2.3. Computation model

The diversion tunnel of a hydropower station of China is taken as the analysis object. The section of the tunnel is circular with a flat bottom. The tunnel buried depth is 200 m and the tunnel excavation diameter is 4.5 m.

To decrease the number of model elements, the buried depth can be divided into two parts of h and H_1, as shown in Fig. 3. In Part I, h represents the depth from the ground level to the upper boundary in the improved model. In Part II, H_1 represents the depth from the upper boundary to the tunnel center. To substitute the gravity of overlying rock mass in Part I, an equivalent distributed pressure P is applied on the upper boundary:

$$P = \gamma h \tag{3}$$

where γ is the overburden rock bulk density of the rock in N·m^{-3}.

Meanwhile, in the improved model, H_2 represents the depth from the tunnel center to the model bottom and H_3 represents the width from the tunnel center to the lateral boundary. Around the tunnel boundary, the minimum of the mesh size is 0.1 m along the radial direction. The opening diameter is approximate 45 times of the mesh size around the tunnel boundary and the results under this computational accuracy can be rational and reliable (Zhao and Janutolo, 2012, Farias et al., 2004).

Then, the upper boundary is free with vertical freedom while the vertical movement of the lower boundary is restricted. The horizontal movements normal to the other boundary are being restricted. As shown in Fig. 4, the longitudinal dimension of the model is H_4, and H_0, the longitudinal distance from the beginning of excavation to the monitoring section, represents the location of the monitoring section. Additionally, around the excavation boundary, monitoring points are located at the crown, the sidewall and the bottom in Fig. 4.

In this stage, the model longitudinal dimension H_4 is set as 200 m, and the monitoring section located at H_0 = 25 m. The main physical–mechanical parameters of the rock mass are a Young's modulus E = 5 GPa, a Poisson's ratio υ = 0.3, a cohesion c = 0.7 MPa, a friction angle φ = 40.36°, a density ρ = 2599 kg/m^3 and a tensile strength σ^t = 2.5 MPa. Moreover, it is worth noting that the rock mass is assumed to be dry and ground water is not considered in this study.

2.4. Simulation procedure

Three-dimensional simulation of tunneling started as a simplified single-step approach (Lee and Rowe, 1991). However, the most popular trend in recent years has been to use the step-by-step procedure (Mollon et al., 2013; Migliazza et al., 2009; Mroueh et al., 2008; Phienwej and Hong et al., 2006; Kasper et al., 2004; Swoboda et al., 2004; Melis et al.,

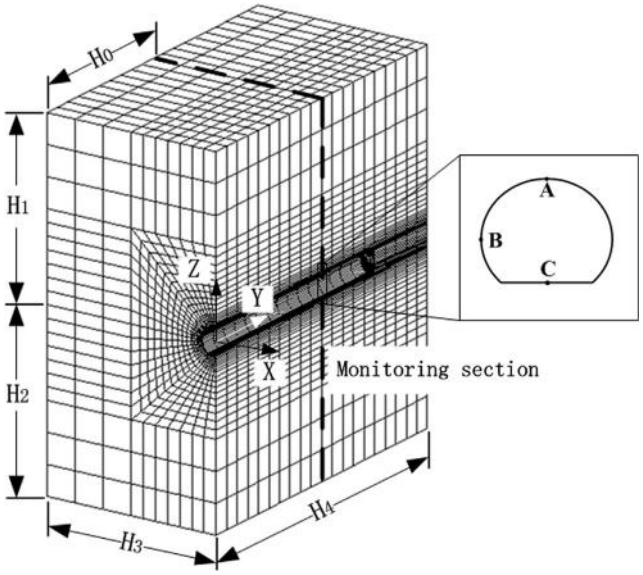

Fig. 4. Computation model.

2002). The later procedure has been adopted in this study. Accordingly, the each excavation step, namely the advancement of the tunnel face in each step, is designed as 2.5 m.

2.5. Lateral stress coefficients and computation schemes

Under the condition of in-situ stress field, the tunnel deformation shape depends mostly on the ratio of lateral stress to vertical one, as shown in Fig. 5. For a circular tunnel, when the lateral stress perpendicular to tunnel axis is less than the vertical one, the deformed shape of tunnel section will be similar to a horizontal ellipse as well as a vertical ellipse for lateral stress larger than vertical one and an idealized scaled circle for lateral stress equal to vertical stress. Generally the lateral stress coefficients of k_x and k_y are adopted to present the ratios of the lateral stresses to the vertical one. In this study, we consider the lateral stress state at x-direction and y-direction is same, namely k_y is equal to k_x. To cover and compare all situations in Fig. 5, four separate schemes are designed: (1) $\sigma_x < \sigma_z$, $k_x = 0.43$ in scheme C1, (2) $\sigma_x < \sigma_z$, $k_x = 0.7$ in scheme C2, (3) $\sigma_x = \sigma_z$, $k_x = 1.0$ in scheme C3 and (4) $\sigma_x > \sigma_z$, $k_x = 1.5$ in scheme C4.

3. Influence of the model transversal extents

The simulation results with $H_1 = 200$ m, $H_2 = H_3 = 12D$ and $H_4 = 200$ m for schemes C1–C4 are adopted as the benchmark in this study. From the results we can find that all the schemes have developed the steady-state solution, as shown in Fig. 6.

The calculation errors of the excavation displacements for the models with less H_1, H_2 and H_3 can be defined by Eq. (4), which represents the bias between the results in each scheme and the reference value.

$$w = \frac{|S_i - S_e|}{S_e} \times 100\% \tag{4}$$

where S_i is the displacement of the monitoring point; S_e is the benchmark value of displacement at the monitoring point.

Meanwhile, with the change of the model extent in different direction, there is great difference on the sensitivity of the different monitoring point. For instance, adjusting the extent of the upper boundary, H_1, the results of the monitoring point at the tunnel crown, A, present more drastic fluctuation than other points. Consequently, to consider the results of different point in a comprehensive approach, the average errors $\bar{w}$ of the monitoring points A, B and C are taken as the fitting curve reference.

$$\bar{w} = (w_A + w_B + w_C)/3 \tag{5}$$

where w_A, w_B and w_C, respectively, represent the computation error for points A, B and C.

3.1. Influence of H_1 on excavation deformation

In the section H_1 will decrease from 12D to 3D while $H_2 = H_3 = 12D$ and $H_4 = 200$ m. The average displacement error $\bar{w}$ can be expressed as a power function of H_1/D as Eq. (6).

$$\bar{w} = a(H_1/D)^b \tag{6}$$

where a and b are parameters for fitting curves as shown in Fig. 7.

The least squares method (Ju, 1998) is used to fit curves in Fig. 7 and the determination coefficient R^2 is employed to comment the fitting reliability. From Fig. 7 we can find that the computation errors yield steady increasing when H_1 decreases from 12D to 6D for all schemes. When H_1 decreases from 6D to 3D, the computation errors increase dramatically from 2.03% to 8.21% for scheme C1, from 1.82% to 7.94% for scheme C2, from 1.29% to 6.96% for scheme C3 and from 0.48% to 4.87% for scheme C4. Meanwhile the Eq. (6) can meet well with the average computation errors.

3.2. Influence of H_2 on excavation deformation

In the section H_2 will decrease from 12D to 3D while $H_1 = H_3 = 12D$ and $H_4 = 200$ m. The average displacement computation error $\bar{w}$ can be expressed as a power function of H_2/D as Eq. (7).

$$\bar{w} = c(H_2/D)^d \tag{7}$$

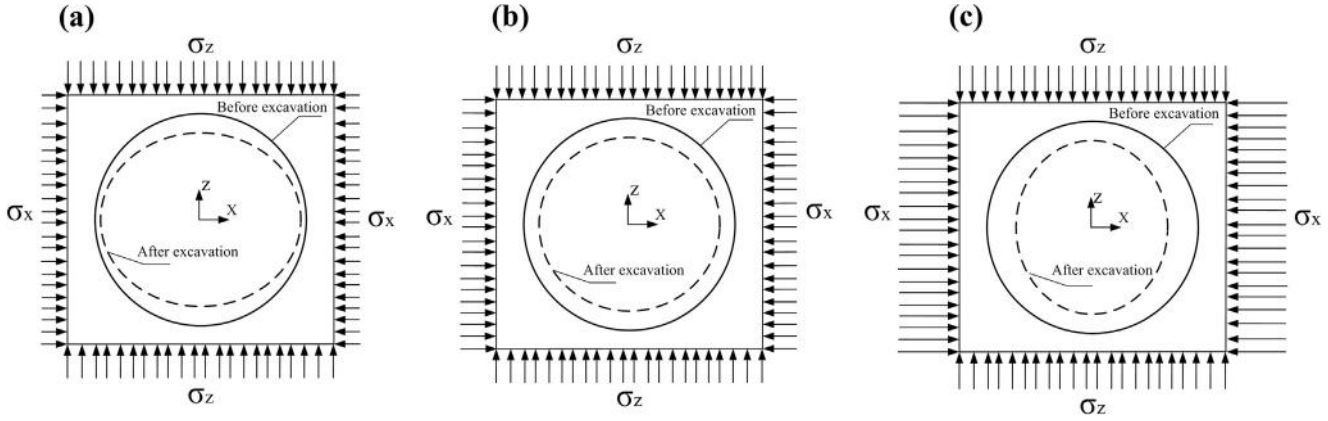

Fig. 5. Deformation of tunnel excavation, (a) $\sigma_x < \sigma_z$, (b) $\sigma_x = \sigma_z$ and (c) $\sigma_x > \sigma_z$.

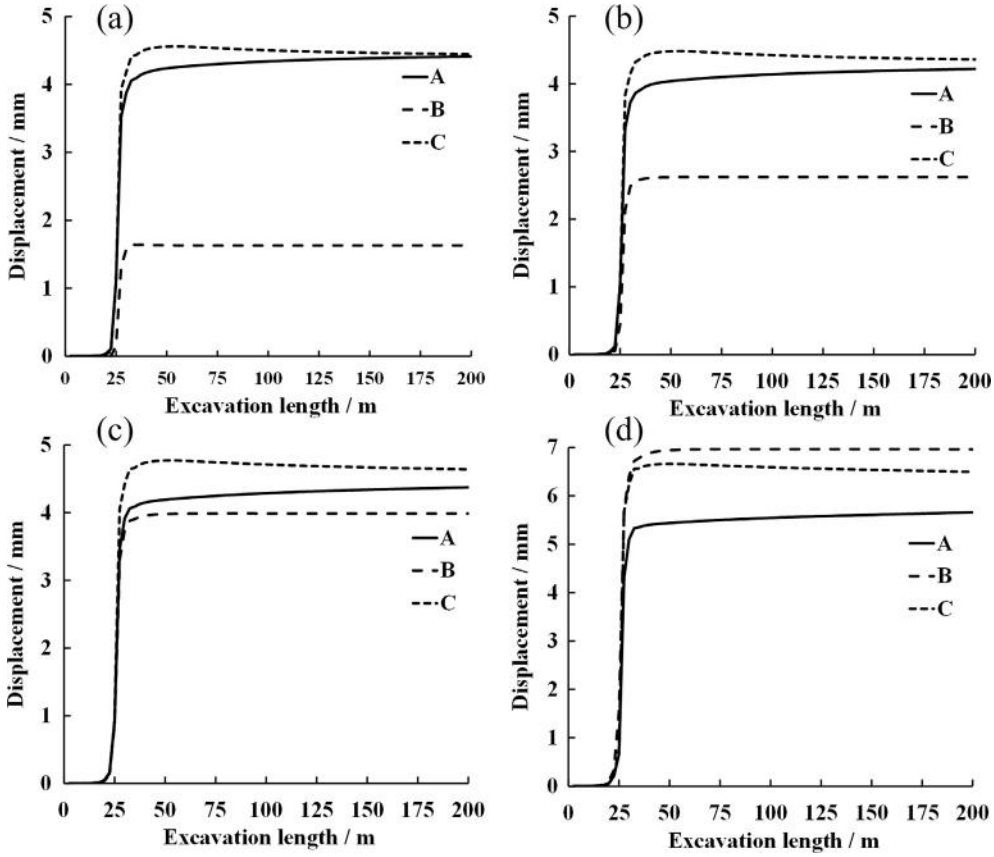

Fig. 6. Deformation profile along with tunneling with $H_1 = 200$ m, $H_2 = H_3 = 12$D and $H_4 = 200$ m,(a) scheme C1, (b) scheme C2, (c) scheme C3 and (d) scheme C4.

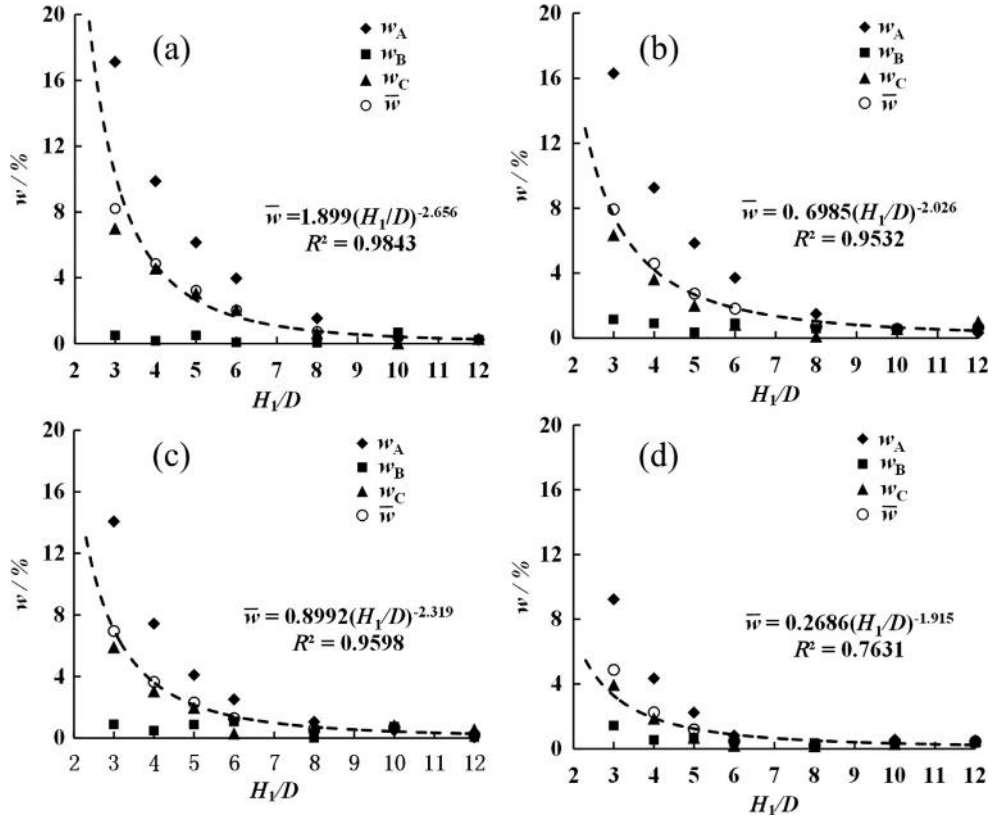

Fig. 7. The computational errors of displacement with $H_2 = H_3 = 12$D and $H_4 = 200$ m, (a) scheme C1, (b) scheme C2, (c) scheme C3 and (d) scheme C4.

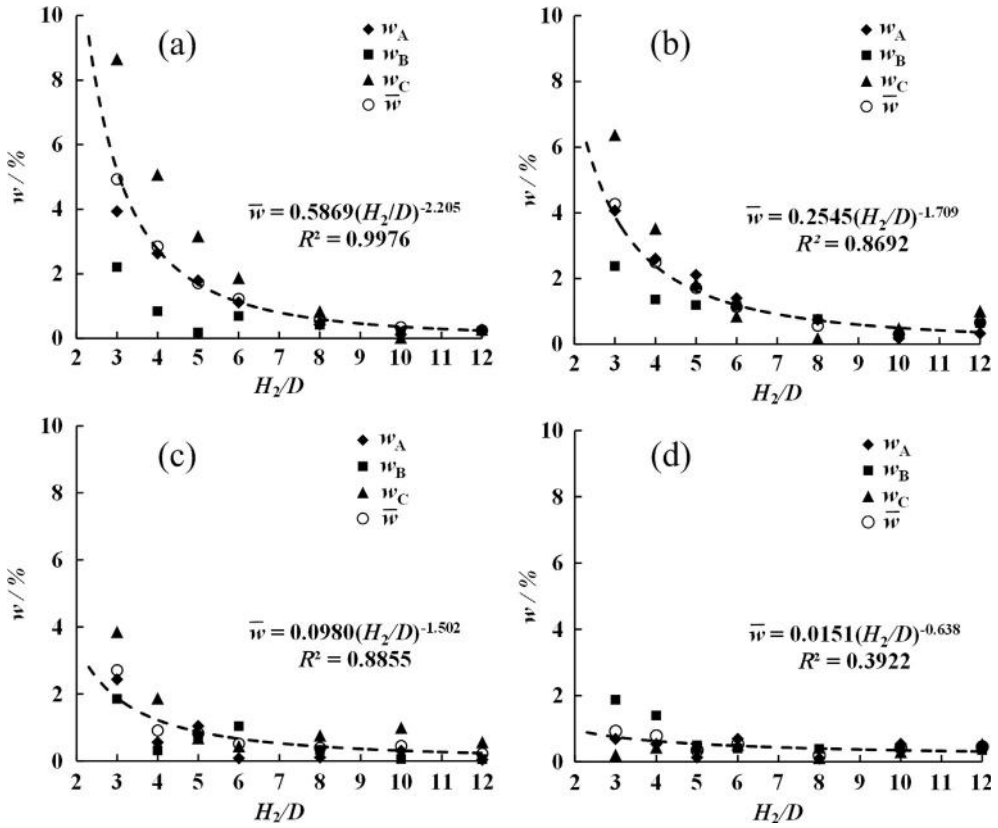

Fig. 8. The influence of H_2 on the displacement computational errors with $H_1 = H_3 = 12D$ and $H_4 = 200$ m, (a) scheme C1, (b) scheme C2, (c) scheme C3 and (d) scheme C4.

where c and d are parameters for fitting curves as shown in Fig. 8.

From Fig. 8 we can find that the computation errors yield steady increasing when H_2 decreases from 12D to 6D for all schemes. When H_2 decreases from 6D to 3D, the average computation errors increase dramatically from 1.23% to 4.93% for scheme C1, from 1.14% to 4.27% for scheme C2, from 0.52% to 2.71% for scheme C3 and from 0.53% to 0.92% for scheme C4.

3.3. Influence of H_3 on excavation deformation

In the section H_3 will decrease from 12D to 3D while $H_1 = H_2 = 12D$ and $H_4 = 200$ m. The average displacement error $\bar{w}$ can be expressed as an exponential function of H_3/D as Eq. (8).

$$\bar{w} = je^{f(H_3/D)} \tag{8}$$

where j and f are parameters for fitting curves as shown in Fig. 9.

From Fig. 9 we can find that the computation errors yield steady increasing when H_3 decreases from 12D to 8D for all schemes. When H_3 decreases from 8D to 3D, the average computation errors increase dramatically from 1.81% to 10.63% for scheme C1, from 1.77% to 9.79% for scheme C2, from 1.64% to 10.59% for scheme C3 and from 1.32% to 10.54% for scheme C4.

4. Transverse extent of model

From the above mentioned results we can find that the computation errors can be expressed as a compound function of H_1, H_2, and H_3 consisting Eq. (6), Eq. (7) and Eq. (8). After the constant term of $\boldsymbol{g}$ is added the compound function can be expressed as Eq. (9).

$$\bar{w} = a(H_1/D)^b + c(H_2/D)^d + je^{f(H_3/D)} + g \tag{9}$$

As the minimum model is based on the minimum transverse section area of model multiplied by the tunnel length, the model transverse section area is proposed as the evaluation index of model size when the element sizes are kept same. Then the minimum transverse extent could be yielded after Eq. (10) when the allowable value $[w]$ of the computation error $\bar{w}$ is given.

$$\begin{cases} A_{op} = Min[2H_3 \times (H_1 + H_2)] \\ \bar{w} = f(H_1/D, H_2/D, H_3/D) \leqslant [w] \end{cases} \tag{10}$$

We choose the allowable value $[w]$ as 5% in this study, which is relatively conservative and can be adjusted with the requirement in engineering (Payton et al., 2003). Then the optimum transverse extents can be yielded for scheme C1 as $H_1 = 6.85D$, $H_2 = 5.56D$ and $H_3 = 6.63D$, for scheme C2 as $H_1 = 6.45D$, $H_2 = 5.19D$ and $H_3 = 6.68D$, for scheme C3 as $H_1 = 5.45D$, $H_2 = 4.00D$ and $H_3 = 6.50D$, for scheme C4 as $H_1 = 4.38D$, $H_2 = 3.00D$ and $H_3 = 5.93D$. And the according parameters are listed in Table 2.

5. Discussion

After Table 2, we choose $H_1 = 31.5$ m (7D), $H_2 = 27$ m (6D) and $H_3 = 31.5$ m (7D) as the universal reference for model transverse extent. Different geological conditions are employed to verify the model extent reference in this study. Three different types of rock mass are considered, ranging from the hard rock to the soft rock, and the material parameters are listed in Table 3.

From the results we can find that the maximum average calculation error of point A, B and C in these simulations is 4.74% arises in T3 with lateral coefficient as 0.54. That is said the model transverse extents of $H_1 = 7D$, $H_2 = 6D$ and $H_3 = 7D$ can be adopted as the universal reference (see Table 4).

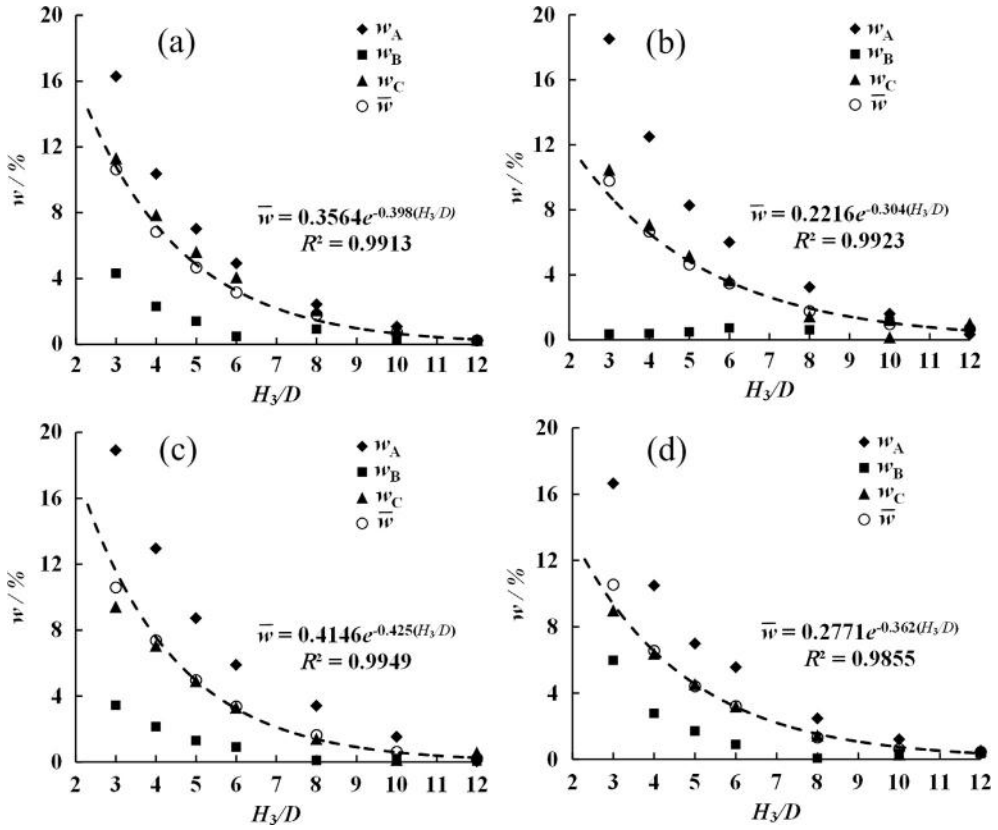

Fig. 9. The influence of H_3 on the displacement computational errors with $H_1 = H_2 = 12D$ and $H_4 = 200$ m, (a) scheme C1, (b) scheme C2, (c) scheme C3 and (d) scheme C4.

Table 2
Fitting parameters for optimal transverse extent of model.

Schemes	Parameters								[w]	H_1/D	H_2/D	H_3/D	A_{op}/D^2
	a	b	c	d	j	f	g	$\sum \delta_i^2/\times 10^{-6}$					
C1	0.5899	−1.7263	0.4217	−1.9259	0.3397	−0.3886	−1.2643	3.53	5%	6.85	5.56	6.63	164.48
C2	0.7630	−2.0408	0.3757	−1.9992	0.2783	−0.3507	−0.7762	3.08	5%	6.45	5.19	6.68	155.36
C3	0.8870	−2.3227	1.9697	−4.0303	0.3304	−0.3776	−0.2974	2.02	5%	5.45	4.00	6.50	122.94
C4	1.6073	−3.2212	0.0221	−0.3397	0.3725	−0.4272	−0.3994	3.79	5%	4.38	3.00	5.93	87.51

Table 3
Material parameters of rock mass.

Discussions	Material parameters					
	Young's modulus E/Gpa	Poisson's ratio ν	cohesion c/MPa	friction angle $\varphi/^\circ$	density ρ/kg·m^{-3}	tensile strength σ^t/MPa
T1	8	0.23	0.95	45	2681	3.5
T2	5	0.30	0.70	40.36	2599	2.5
T3	3	0.35	0.20	30.96	2497	1.25

Table 4
Calculations errors summary for diverse rock mass.

Discussions	Lateral coefficients	Displacement S_i, mm ($H_1 = 7D$, $H_2 = 6D$ and $H_3 = 7D$)			Benchmark of displacement, S_e, mm ($H_1 = 200$ m, $H_2 = 12$D and $H_3 = 12$D)			$\bar{w}$/%
		A	B	C	A	B	C	
T1	0.33	2.61	0.28	2.69	2.73	0.28	2.58	3.55
	0.70	2.33	1.15	2.51	2.45	1.17	2.43	3.28
	1.00	2.21	1.97	2.47	2.33	1.96	2.39	3.11
	1.50	2.28	3.61	2.82	2.40	3.59	2.74	2.85
T2	0.43	4.63	1.64	4.26	4.41	1.63	4.44	3.25
	0.70	4.46	2.65	4.21	4.22	2.62	4.36	3.33
	1.00	4.63	3.94	4.47	4.38	3.99	4.64	3.52
	1.50	5.90	6.93	6.32	5.66	6.96	6.50	2.52
T3	0.54	17.00	16.58	15.45	18.23	16.82	14.60	4.74
	0.70	19.18	18.32	17.64	20.35	18.55	16.82	4.00
	1.00	25.01	23.37	23.18	25.92	23.35	22.31	2.50
	1.50	40.05	34.48	37.96	40.21	33.76	36.31	2.27

6. Conclusions

This paper focuses on the influence of transverse model extent on tunnel deformation. After a steady-state developed, the computation errors are carried out based on the results of $H_1 = 200$, $H_2 = H_3 = 12$D and $H_4 = 200$ m, which could be expressed as a power function of H_1/D as well as H_2/D, as an exponential function of H_3/D. The minimum area of model transverse section can be yielded when an allowable error is introduced into the proposed compound function of H_1/D, H_2/D and H_3/D. In this study, the allowable error is set as 5%, which is acceptable

and can be adjusted. When the allowable error is 5%, the model transverse extents of H_1 = 7D, H_2 = 6D and H_3 = 7D are proposed as the universal reference and verified with diverse rock class.

Acknowledgements

The authors wish to acknowledge the financial support of the National Key Research and Development Program of China (2016YFC0401803) and the National Natural Science Foundation of China (Nos. 51579194 & 51879207).

References

Augarde, C.E., Burd, H.J., Houlsby, G.T., 1998. Some Experiences of Modelling Tunnelling in Soft Ground Using Three-Dimensional Finite Elements. Springer Vienna.
Barla, G., Barla, M., Bonini, M., 2005. Two and three dimensional modelling and monitoring of the Metro Torino. In: 11th International Conference of IACMAG. Turin, Italy, pp. 743–752.
Belytschko, T., Hughes, T.J.R., Burgers, P., 1983. Computational Methods for Transient Analysis. Elsevier Science Pub. Co.
Burd, H.K., Houslby, G.T., Augarde, C.E., et al., 2000. Modelling tunnellmg-induced settlement of masonry buildings. Geotechnical Engineering 143 (1), 17–29.
Cai, M., 2008. Influence of stress path on tunnel excavation response-Numerical tool selection and modeling strategy. Tunn. Undergr. Space Technol. 23 (6), 618–628.
Dasari, G.R., Rawlings, C.G., Bolton, M.D., 1996. Numerical modelling of a NATM tunnel construction in London Clay. Int. Symp. on Geotechnical Aspects of Underground Construction in Soft Ground. Balkema, Rotterdam.
Dias, D., Kastner, R., Maghazi, M., 2000. Three-dimensional simulation of slurry shield tunnelling. In: Int. Symp. on Geotechnical Aspects of Underground Construction in Soft Ground. Balkema, Rotterdam, pp. 351–356.
Do, N., Dias, D., Oreste, P., et al., 2014. Three-dimensional numerical simulation for mechanized tunnelling in soft ground: the influence of the joint pattern. Acta Geotech. 9 (4), 673–694.
Doležalová, M., 2002. Approaches to numerical modelling of ground movements due to shallow tunnelling. In: Int. Symp. Soil Structure Interaction in Urban Civil Engineering. Swiss Federal Institute of Technology ETH Zurich, Zurich, pp. 365–373.
Farias, M.M.D., Júnior, Álvaro Henrique Moraes, Assis, A.P.D., 2004. Displacement control in tunnels excavated by the NATM: 3-D numerical simulations. Tunnell. Undergr. Space Technol. Incorp. Trenchless Technol. Res. 19 (3), 283–293.
Franzius, J.N., Potts, D.M., 2005. Influence of mesh geometry on three-dimensional finite-element analysis of tunnel excavation. Int. J. Geomech. 5 (3), 256–266.
Galli, G., Grimaldi, A., Leonardi, A., 2004. Three-dimensional modelling of tunnel excavation and lining. Comput. Geotech. 31 (3), 171–183.
Guedes, P.F.M., Santos, Pereira C., 2000. The role of the soil K0 value in numerical analysis of shallow tunnels. In: Int. Symp. On Geotechnical Aspects of Underground Construction in Soft Ground. Balkema, Rotterdam, pp. 379–384.
Itasca, C.G., 2002. FLAC3D Fast Lagrangian Analysis of Continua in 3-D. Itasca Consulting Group Inc., Minneapolis Minn.
Jenck, O., Dias, D., 2003. Numerical analysis of the volume loss influence on building during tunnel excavation (Numerical analysis of the volume loss influence on building during tunnel excavation). In: Third International FLAC Symposium—FLAC and FLAC3D numerical modelling in geomechanics. Sudbury,Canada.
Ju, S.H., 1998. Simulating three-dimensional stress intensity factors by the least-squares method. Int. J. Numer. Meth. Eng. 43 (8), 1437–1451.
Kasper, T., Meschke, G., 2004. A 3D finite element simulation model for TBM tunnelling in soft ground. Int. J. Numer. Anal. Meth. Geomech. 28 (14), 1441–1460.
Katzenbach, R., Breth, H., 1981. Nonlinear 3-d analysis for natm in frankfurt clay. In: Proceedings of 10th International Conference on Soil Mechanics and Foundation Engineering. Balkema, Rotterdam, pp. 315–318.
Komiya, K., Soga, K., Akagi, H., et al., 1999. Finite element modelling of excavation and advancement processes of a shield tunnelling machine. Soils Found. 39 (3), 37–52.
Lambrughi, A., Medina Rodríguez, L., Castellanza, R., 2012. Development and validation of a 3D numerical model for TBM–EPB mechanised excavations. Comput. Geotech. 40, 97–113.
Lee, G.T.K., Ng, C.W.W., 2002. Three-dimensional analysis of ground settlements due to tunnelling: role of K0 and stiffness anisotropy. In: In the International Symposium on Geotechnical Aspects of Underground Construction in Soft Ground. Spécifique, Lyon, pp. 617–622.
Lee, K.M., Rowe, R.K., 1991. An analysis of three-dimensional ground movements: the Thunder Bay tunnel. Can. Geotech. J. 28 (1), 25–41.
Liu, H.Y., Small, J.C., Carter, J.P., et al., 2009. Effects of tunnelling on existing support systems of perpendicularly crossing tunnels. Comput. Geotech. 36 (5), 880–894.
Maranha, J.R., Neves, E.M.D., 2000. 3D analysis of ground displacements due to the construction of lisbon underground. Proceedings of the International Conference on Geotechnical & Geological Engineering. Melbourne.
Melis, M., Medina, L., Rodriguez, J., 2002. Prediction and analysis of subsidence induced by shield tunnelling in the Madrid Metro extension. Can. Geotech. J. 39 (6), 1273–1287.
Migliazza, M., Chiorboli, M., Giani, G.P., 2009. Comparison of analytical method, 3D finite element model with experimental subsidence measurements resulting from the extension of the Milan underground. Comput. Geotech. 36 (1), 113–124.
Mollon, G., Dias, D., Soubra, A.H., 2013. Probabilistic analyses of tunneling-induced ground movements. Acta Geotech. 8 (2), 181–199.
Mroueh, H., Shahrour, I., 2008. A simplified 3D model for tunnel construction using tunnel boring machines. Tunn. Undergr. Space Technol. 23 (1), 38–45.
Payton, M.E., Greenstone, M.H., Schenker, N., 2003. Overlapping confidence intervals or standard error intervals: What do they mean in terms of statistical significance. J. Insect Sci. 3 (1), 34.
Phienwej, N., Hong, C.P., Sirivachiraporn, A., 2006. Evaluation of ground movements in EPB-shield tunnelling for Bangkok MRT by 3D-numerical analysis. Tunn. Undergr. Space Technol. 21 (3–4), 273.
Shin, J.H., Potts, D.M., Zdravković, L., 2002. Three-dimensional modelling of NATM tunnelling in decomposed granite soil. Geotechnique 52 (3), 187–200.
Su, K., Chang, Z.H., Cui, J.P., et al., 2016. Study of model longitudinal range in numerical simulation of deep tunnel excavations. Rock Soil Mech. 37 (S2), 706–714.
Swoboda, G., Kenawi, M., Ramadan, E., 2004. Numerical investigation of TBM tunnelling in consolidated clay. Tunn. Undergr. Space Technol. 19 (4–5), 459.
Tang, D.K.W., Lee, K.M., Ng, C.W.W., 2000. Stress paths around a 3-D numerically simulated NATM tunnel in stiff clay. In: Proc. of the International Sym-posium on Geotechnical Aspects of Underground Construction in Soft Ground. Balkema, Rotterdam, pp. 443–449.
Vermeer, P.A., Bonnier, P.G., Möller, S.C., 2002. On a smart use of 3D-FEM in tunnelling. Proceedings of the 8th International Symposium NUMOG VIII. Rome, Italy.
Zhang, W., Goh, A.T.C., 2012. Reliability assessment on ultimate and serviceability limit states and determination of critical factor of safety for underground rock caverns. Tunn. Undergr. Space Technol. 32 (11), 221–230.
Zhang, W.G., Goh, A.T.C., 2015. Regression models for estimating ultimate and serviceability limit states of underground rock caverns. Eng. Geol. 188, 68–76.
Zhao, K., Janutolo, M., 2012. A completely 3D model for the simulation of mechanized tunnel excavation. Rock Mech. Rock Eng. 45 (4), 475–497.